

A Compilation Framework for Quantum Circuits with Mid-Circuit Measurement Error Awareness

Ming Zhong[†], Zhemin Zhang[†], Xiangyu Ren[‡], Chenghong Zhu[§], Siyuan Niu[¶], Zhiding Liang^{†*}

[†]The Chinese University of Hong Kong, [‡]University of Edinburgh

[§]The Hong Kong University of Science and Technology, [¶]University of Central Florida

Abstract—Mid-circuit measurement (MCM) provides the capability for qubit reuse and dynamic control in quantum processors, enabling more resource-efficient algorithms and supporting error-correction procedures. However, MCM introduces several sources of error, including measurement-induced crosstalk, idling-qubit decoherence, and reset infidelity, and these errors exhibit pronounced qubit-dependent variability within a single device. Since existing compilers such as the Qiskit-compiler and QR-Map (the state-of-art qubit reuse compiler) do not account for this variability, circuits with frequent MCM operations often experience substantial fidelity loss.

In this paper, we propose MERA, a compilation framework that performs MCM-error-aware layout, routing, and scheduling. MERA leverages lightweight profiling to obtain a stable per-qubit MCM error distribution, which it uses to guide error-aware qubit mapping and SWAP insertions. To further mitigate MCM-related decoherence and crosstalk, MERA augments as-late-as-possible scheduling with context-aware dynamic decoupling. Evaluated on 27 benchmark circuits, MERA achieves 24.94% – 52.00% fidelity improvement over the Qiskit compiler (optimization level 3) without introducing additional overhead. On QR-Map-generated circuits, it improves fidelity by 29.26% on average and up to 122.58% in the best case, demonstrating its effectiveness for dynamic circuits dominated by MCM operations.

I. INTRODUCTION

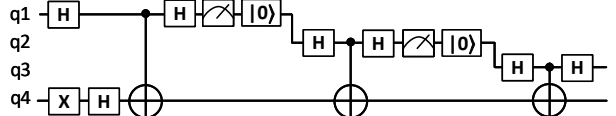
Quantum computing is regarded as a promising paradigm for solving classically intractable problems [10], [4], [7]. However, current quantum hardware remains in the Noisy Intermediate-Scale Quantum (NISQ) era, where limited qubit counts and multiple noise sources hinder the reliable quantum computation [18], [26]. To alleviate qubit scarcity, modern superconducting processors such as IBM [14] and Google quantum processors [8] incorporate mid-circuit measurement (MCM) operations, enabling dynamic circuits where qubits can be measured, reset, and reused during computation. Unlike static circuits, dynamic circuits perform conditional operations based on MCM outcomes, improving resource efficiency and supporting error correction without increasing qubit count. MCM also serves as an important enabler for fault-tolerant quantum error correction, where stabilizer measurements and ancilla resets are repeatedly performed. Moreover, MCM-based conditional control and qubit recycling have been proposed to facilitate distributed quantum computing. Several studies have leveraged MCM mechanisms, including qubit reset, to enable qubit reuse and improve resource efficiency in quantum computation [3], [12], [17]. A typical example is

the Bernstein–Vazirani (BV) circuit [2] in Fig. 1a, where two MCM stages allow a four-qubit circuit to run on only two qubits, greatly reducing qubit demand. Another representative use is in Repeat-Until-Success (RUS) circuits in Fig. 1b, which iteratively execute probabilistic subroutines until a success condition is met, and are widely used in quantum machine learning [29], [25].

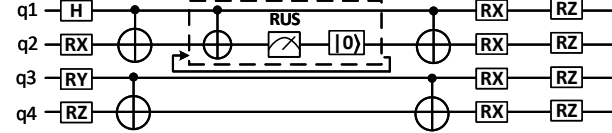
NISQ superconducting processors exhibit non-negligible MCM errors. Here, an MCM error means that after performing a measurement and then a conditioned reset, the post-reset state is incorrect. These MCM errors arise from several factors, including readout errors, measurement-induced crosstalk, and reset infidelity [11]. Moreover, unlike neutral-atom qubits, superconducting qubits are artificial in nature, leading to significant device-level variation even within a single chip, such as coherence times, frequency detuning ranges, and other device-level characteristics. Owing to this inherent ‘heterogeneity’ in superconducting processors, we further investigate the qubit-specific variation of MCM errors. As shown in Fig. 2a, profiling on the 127-qubit IBM Eagle processor shows MCM error rates ranging from 0.05% to 42.58% (average 3.42%). Similarly, results from the 156-qubit IBM Heron processor in Fig. 2b show a range of 0% to 14.04% (average 1.19%). This variability occurs both across qubits within a device and across different devices; since MCM operations underpin qubit reuse and RUS circuits, mapping MCM qubits to high-error locations can markedly reduce fidelity. Yet mainstream compilers such as Qiskit-compiler [13] and state-of-art (SOTA) qubit-reuse compilers like CaQR [12] and QR-Map [17] ignore MCM errors and such outstanding heterogeneity among superconducting qubits, motivating a compilation framework that models MCM error heterogeneity to improve reliability.

In this paper, we first profile MCM errors on real superconducting processors using a simple yet effective method, obtaining a per-qubit error distribution that remains stable for at least 24 hours according to our temporal analysis. We then propose MERA, an MCM-error-aware compiler that incorporates MCM-error modeling into the layout and routing stages, enabling MCM-error-aware qubit mapping and SWAP insertion. During scheduling, it applies as-late-as-possible (ALAP) scheduling and performs context-aware dynamic decoupling (CADD) [1] to mitigate decoherence and measurement-induced crosstalk introduced by MCM operations, thereby further improving fidelity. While this work

*Corresponding Author: zliang@cse.cuhk.edu.hk.



(a) A qubit-reuse circuit for Bernstein-Vazirani (BV) algorithm.



(b) A 4-qubit circuit with repeat-until-success (RUS) operation.

Fig. 1: Representative circuits containing MCM operations.

focuses on superconducting platforms where qubit ‘heterogeneity’ is most evident, MERA could be extended to other qubit technologies by integrating their hardware-specific characteristics.

To summarize, this work makes the following contributions:

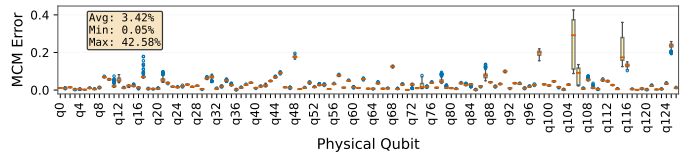
- **An MCM-error-aware compiler** named MERA integrates MCM error modeling into layout, routing, and scheduling. It performs lightweight profiling to capture a per-qubit MCM error distribution that typically persists for over 24 hours, avoiding frequent re-profiling. MERA leverages this error distribution and together with CADD to mitigate MCM induced errors, thereby effectively reducing fidelity loss in circuits involving MCM operations.
- **Comprehensive evaluation** on 27 benchmark circuits, including 8 RUS, 17 qubit-reuse, and 2 benchmarks including MCM operations from QASMBench [20]. The Qiskit-compiler (v2.1.2, optimization level 3) serves as the baseline, and QR-Map [17], the SOTA qubit-reuse compiler, is included for comparison. Results show that MERA improves circuit fidelity by 24.94% – 52.00% on average over Qiskit-compiler without adding additional SWAP overhead. By post-processing circuits generated by QR-Map, MERA further enhances fidelity by 29.26% on average, confirming MERA’s effectiveness on circuits with MCM operations.

II. BACKGROUND

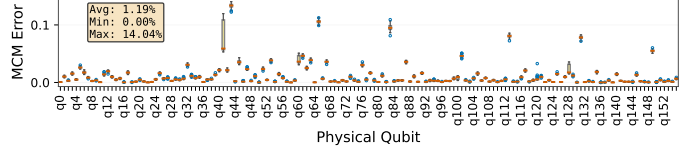
A. Middle-circuit-measurement

Mid-circuit measurement (MCM) performs measurements during circuit execution rather than only at the end of the circuit, enabling conditional resets based on intermediate outcomes. By collapsing and reinitializing qubit states, MCM reduces circuit entropy and underpins fault-tolerant quantum computing and dynamic circuits with qubit reuse [11]. After measurement, a qubit can be **reset** to a known state (typically $|0\rangle$) and reassigned to serve as another logical qubit, thereby improving hardware utilization [3].

In Fig. 1a, a 4-qubit BV circuit is optimized via MCM-based qubit reuse. By measuring and resetting q_1 after each two qubit gate with q_4 , the same qubit is reused three times, eliminating q_2 and q_3 and reducing qubit count. Nevertheless, effective qubit reuse relies on high-fidelity MCM



(a) The IBM Eagle quantum processor.



(b) The IBM Heron quantum processor.

Fig. 2: MCM error distributions for quantum processors.

operations; otherwise, frequent MCMs can significantly degrade overall circuit fidelity.

B. Error sources of MCM

Errors introduced by MCM can be attributed to several sources. First, measurement-induced crosstalk can disturb neighboring qubits. Second, during the long measurement window, unmeasured qubits remain idle and accumulate decoherence errors. Third, the measurement process itself can yield readout errors, misreporting qubit states [11]. For reset operations within MCM, the process involves driving the qubit from $|1\rangle$ to $|0\rangle$ through a bit-flip transition. Reset errors primarily stem from failures in this transition, where the qubit is not successfully restored to the expected ground state.

Our experiments reveal substantial variation in MCM errors across physical qubits on 127- and 156-qubit IBM devices: while some qubits exhibit near-perfect fidelity (MCM error = 0.00%), others show much higher MCM error rates up to 42.58%, underscoring the need for qubit-aware layout and compilation strategies.

Moreover, prior work shows that the fidelity of reset operations strongly depends on the qubit’s pre-reset state: the greater the overlap with $|1\rangle$, the lower the post-reset fidelity, and vice versa. Applying a second reset pulse typically improves fidelity, while additional repetitions yield diminishing returns, with the optimal number of pulses varying across qubits. Concurrent resets contribute negligibly to total error, indicating that reset infidelity is mainly dominated by qubit-specific imperfections [3]. However, the limitation of this prior work [3] is that it attributes MCM errors entirely to reset errors, while neglecting the influence of readout, crosstalk, and decoherence errors within MCM.

C. Motivation

MCM is particularly essential in scalable algorithms involving error correction and distributed quantum computing emphasized by qubits reuse. However, MCM introduces errors from MCM-induced crosstalk, decoherence, readout error, and reset infidelity (leakage included). Based on our experiments on real superconducting processors, the IBM’s devices, we observe significant heterogeneity in MCM errors

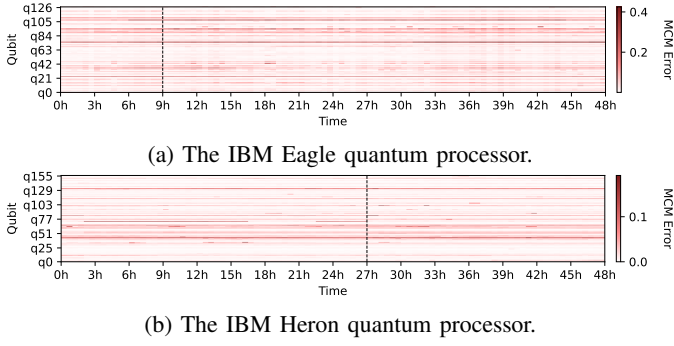


Fig. 3: Stability of MCM errors in quantum processors.

across qubits due to device-level characteristics. This observation highlights the need for an MCM-error-aware compiler. Existing works [17], [12], [3] on reset-aware compilation mainly optimize qubit reuse but overlook spatial MCM error variations. Blindly mapping high-intensity MCM operations to high-error qubits can severely degrade fidelity and reliability. Our work address the gap by analyzing MCM error, and integrate the awareness and mitigation of different parts of MCM errors into layout, routing, and scheduling to enhance the robustness of quantum compilation.

III. MCM ERROR PROFILING

A. Profiling Approach

To systematically evaluate MCM errors on large superconducting quantum processors while minimizing execution overhead, we design a simple and hardware-agnostic MCM error profiling approach based on the following operation sequence for each single qubit:

$$|0\rangle \xrightarrow{X \text{ Gate}} |1\rangle \xrightarrow{\text{MCM with Reset}} \text{Measure} \Rightarrow P(|0\rangle)$$

This procedure measures the probability $P(\text{Measurement} = |0\rangle)$ after the MCM operation (with reset) of each qubit, providing a direct estimate of its success probability. Specifically, each qubit is first initialized to the $|1\rangle$ using an X gate, then middle-circuit-measured, reset, and finally measured again at the end of the circuit. The experiment is repeated 1,024 shots using the Session API in Qiskit to enable large-scale *parallel execution* and ensure consistent sampling conditions across all physical qubits.

While the existing MCM error profiling method (QIRB [11]) provides precise MCM error rates and can isolate crosstalk-induced errors, its application to large-scale quantum devices incurs substantial experimental cost. In contrast, our method efficiently estimates per-qubit MCM error distributions with far lower cost. Since MERA does not require highly precise or frequently updated MCM errors, minor daily fluctuations are tolerable and have negligible impact on compilation quality, as shown in our evaluation. Consequently, QIRB is more suitable for applications that demand persistently fine-grained error characterization and explicit crosstalk isolation.

B. Profiling Results

We perform full-device MCM error profiling on the 127-qubit IBM Eagle and 156-qubit IBM Heron processors to obtain the per-qubit MCM error distribution. Fig. 2 presents the profiling results, where the orange line denotes the average MCM error of each qubit. On the Eagle processor (Fig. 2a), MCM errors range from 0.05% to 42.58%, with a mean of 3.42%, revealing substantial spatial variability. Several peripheral qubits (e.g., 105 and 115) exhibit notably higher errors, likely due to less frequent calibration or stronger coupling to readout resonators. A similar pattern appears on the 156-qubit Heron processor (Fig. 2b), where errors span 0.00% to 14.04% with an average of 1.19%. As a newer generation, Heron benefits from improved flux-line calibration and reduced ZZ crosstalk via tunable couplers, resulting in lower overall MCM errors. Nevertheless, the per-qubit variance remains significant and cannot be ignored.

C. Temporal Stability of MCM Errors

To evaluate the temporal stability of MCM errors, we repeatedly profiled the Eagle and Heron processors for 48 hours at 0.5-hour intervals and visualized the results as time-series heatmaps. Inspection of the profiling log confirmed that the profiling intervals remained essentially 0.5 hours and were not affected by long-running jobs from other users. As shown in Fig. 3a, certain qubits (e.g., q_{24}, q_{106}) consistently exhibit high MCM error rates, while others (e.g., $q_{47}-q_{64}$) remain low, demonstrating strong heterogeneity. From hour 9 onward, the overall distribution remains largely stable for over 24 hours, with only minor fluctuations (e.g., at q_{43}), and the qubits showing these changes already had elevated errors at hour 9. Thus, a single profiling run provides a reliable MCM error distribution for at least 24 hours, avoiding frequent re-profiling. A similar trend appears in Fig. 3b: over the 0–27 hour period, the Heron processor’s MCM error distribution remains stable and is consistently lower than Eagle’s, consistent with the profiling results in Fig. 2. These temporal results confirm that MCM errors on superconducting processors remain stable for 24 hours or longer, highlighting the value of MCM-error-aware compilation to improve the fidelity of circuits with frequent MCM operations.

IV. MERA: AN MCM-ERROR-AWARE COMPILER

A. Overview of MERA

Fig. 4 summarizes the workflow of MERA. Given a quantum circuit and the measured MCM-error distribution of the target device (Fig. 4(a)), MERA’s compilation process goes through three stages: layout, routing, and scheduling. In the layout stage (Fig. 4(b)), MERA defines a unified cost function that incorporates MCM errors along with distance, two-qubit (2Q), single-qubit (1Q), and readout (RO) errors to guide layout candidate generation and selection. During routing (Fig. 4(c)), MERA employs a two-level ranking strategy built on the SABRE method [21] to route high-intensity MCM qubits onto lower-error physical qubits without increasing SWAP overhead. For scheduling (Fig. 4(d)), MERA applies

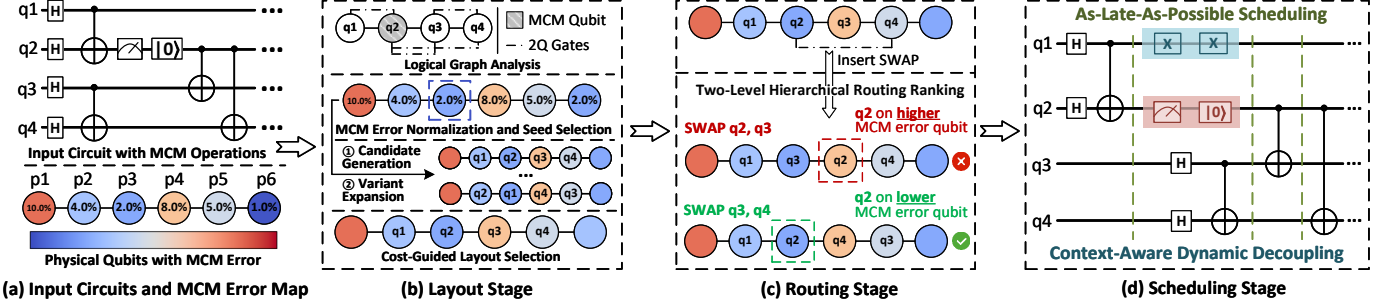


Fig. 4: The workflow of MERA. More MCMs (on q_2), and single- and two-qubit gates (on $q_1 - q_4$) are omitted for brevity.

ALAP scheduling followed by CADD to improve fidelity of circuits with MCM operations.

B. Layout Stage

1) *Logical Graph Analysis*: As shown in Fig. 4(b), MERA first analyzes the input circuit and construct a logical interaction graph $G = (V, E)$, where each logical qubit $q_i \in V$ is a node and each two-qubit gate defines an edge $(q_i, q_j) \in E$. From the circuit schedule, we also extract the MCM operation insensitivity $MCM_Int(q_i)$ of each qubit q_i that involves MCM operation.

$$MCM_Cost(q_i, p_j) = MCM_Int(q_i) \times Err_{MCM}(p_j) \quad (1)$$

Additionally, we model the MCM error cost (MCM_Cost) for each logical–physical mapping using Eq. (1). When a logical qubit q_i is mapped to a physical qubit p_j , its cost is defined as the product of its MCM-operation intensity $MCM_Int(q_i)$ and the empirical MCM error rate $Err_{MCM}(p_j)$. The total circuit-level MCM cost is the sum of these per-qubit MCM cost, linking how frequently each logical qubit performs MCM to the reliability of its mapped physical qubit. This MCM cost design encourages MCM-intensive logical qubits to be placed on physical qubits with lower MCM error.

2) *MCM Error Normalization and Seed Selection*: In this step, MERA selects N_{Seed} physical qubits as seeds for subsequent layout expansion. Unlike the random seeding strategy used in the SABRE [21] layout approach, MERA ranks physical qubits using a normalized composite score that reflects both their error characteristics, including MCM error, two-qubit gate error, readout error, single-qubit gate error, and their connectivity.

$$\widetilde{Err}_{MCM}(p) = \begin{cases} \tau_{MCM}, & Err_{MCM}(p) \leq \tau_{MCM} \\ Err_{MCM}(p), & Err_{MCM}(p) > \tau_{MCM} \end{cases} \quad (2)$$

Specifically, MERA first normalizes the MCM error rates of all physical qubits using the threshold τ_{MCM} in Eq. (2). When a qubit’s MCM error rate falls below this threshold, its contribution to fidelity loss is negligible. Without normalization, the compiler may overemphasize tiny differences in low-error regions and underweight other factors such as distance. Normalization suppresses these sub-threshold variations

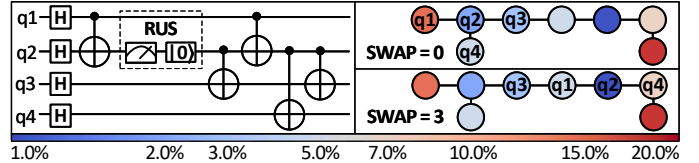


Fig. 5: Layouts with and without MCM error normalization. The 1.0% – 20.0% range in the error map is *nonlinearly scaled* to highlight subtle differences in color contrast.

and restores a balanced weighting among all hardware noise sources in the cost function.

Fig. 5 illustrates this effect on a heavy-hex architecture, showing only part of the coupling map for clarity. For the same input circuit, the top layout maps the MCM qubit q_2 to a well-connected physical qubit with a 2% MCM error rate, while the bottom layout maps it to a less connected qubit with a lower 1% error rate. Despite the smaller MCM error, the latter requires three additional SWAPs, increasing overhead and reducing fidelity. This highlights the importance of MCM error normalization for balancing reliability and connectivity.

$$Score(p) = \alpha(1 - \widetilde{Err}_{MCM}(p)) + \beta(1 - \bar{e}_{2Q}(p)) + \gamma(1 - \bar{e}_{1Q}(p)) + \delta(1 - \bar{e}_{RO}(p)) + \epsilon Conn(p) \quad (3)$$

After MCM error normalization, MERA ranks all physical qubits using Eq. (3) and selects the top N_{Seed} as layout seeds. The scoring function combines connectivity $Conn(p)$ (in-degree) with weighted MCM, two-qubit, single-qubit, and readout error rates ($\bar{e}_{2Q}/\bar{e}_{1Q}/\bar{e}_{RO}$) to form a unified score, prioritizing qubits that offer both low error and high connectivity. For example, in Fig. 4(a), qubit p_6 with a 1.0% MCM error is normalized to 2.0% in Fig. 4(b) and p_3 is selected as the seed due to its better connectivity compared with p_6 .

3) *Layout Candidate Generation and Expansion*: From each seed, MERA performs a breadth-first (BFS) expansion over the hardware coupling graph, exploring candidate physical qubits within 1–2 hops (i.e., direct and second-layer neighbors). Each candidate placement is then evaluated using a layout cost function (Eq. (4)) that extends SABRE’s look-ahead strategy [21], where $look_ahead$ specifies the number of future layers considered.

$$\begin{aligned}
Cost_{\text{Layout}}(L_M) = & w_{\text{dist}} \text{SABRE}(L_M, \text{look_ahead}) + \sum_{(q_i, p_j) \in L_M} \\
& \left[w_{\text{MCM}} \text{MCM_Cost}(q_i, p_j) + w_{2Q} N_{p_j}^{2Q}(L_M) \bar{e}_{2Q}(p_j) + \right. \\
& \left. w_{1Q} N_{p_j}^{1Q}(L_M) \bar{e}_{1Q}(p_j) + w_{\text{RO}} N_{p_j}^{\text{RO}}(L_M) \bar{e}_{\text{RO}}(p_j) \right]
\end{aligned} \quad (4)$$

In Eq. (4), L_M denotes the current logical-to-physical qubit mapping, and the *SABRE* function represents the original front-layer and look-ahead distance heuristic [21]. We extend this cost function by incorporating MCM errors and the 2Q/1Q/RO error rates (\bar{e}_{2Q} , \bar{e}_{1Q} , \bar{e}_{RO}) of each logical–physical pair (q_i, p_j) in L_M , weighted to form a composite cost function. Here, $N^{2Q/1Q/\text{RO}}_{p_j}(L_M)$ denotes the number of corresponding 2Q/1Q/readout operations executed on physical qubit p_j under the layout mapping L_M .

During the BFS expansion for layout candidate generation, let I denote the current partial mapping and (q_u, p_v) the next logical–physical qubit pair to be mapped. Eq. (5) then evaluates the incremental cost of extending the current mapping I by (q_u, p_v) by applying Eq. (4), guiding the BFS expansion for layout generation.

$$\Delta C((q_u, p_v) \mid I) = Cost_{\text{Layout}}(I \cup (q_u, p_v)) \quad (5)$$

The BFS expansion terminates once all logical qubits are mapped to distinct physical qubits, or when no lower-cost neighbor within the 2-hop radius can further reduce the incremental cost ΔC . If termination occurs before full coverage, MERA optionally performs a single shortest-path bridging step to connect the remaining unmapped qubits to the partial layout, ensuring a fully connected and valid mapping. After generating initial candidate mappings, MERA increases layout diversity by generating intra-candidate variants, i.e., reassigning logical–physical pairs within the same selected physical set. For each candidate, variants are created using two reordering rules: (1) MCM-aware reordering: assign logical qubits with higher MCM intensity to physical qubits with lower MCM error; (2) Connectivity-aware reordering: assign logical qubits with higher two-qubit participation to physical qubits with higher connectivity centrality in the hardware coupling graph.

This variant generation broadens the local search around each BFS expansion, improving robustness against local minima and increasing the likelihood of finding a layout with lower cost.

4) *Cost-Guided Layout Selection*: For all generated layout candidates (including variants), MERA computes the global layout cost again using Eq. (4) and selects the layout with the lowest cost as the final mapping result for each layout candidate.

C. Routing Stage

In the routing stage, MERA primarily adopts a *SABRE*-style routing strategy enhanced with a two-level hierarchical

ranking mechanism to balance routing efficiency and MCM error awareness.

Building on the original *SABRE* strategy, MERA generates SWAP candidates from coupling edges connected to the current front-layer 2Q gates, preserving *SABRE*’s locality and efficiency. When no candidate yields a shorter logical-to-physical distance, the routing algorithm falls back to the previous candidate set to maintain routing progress and prevent stalling.

Next, MERA employs a two-level hierarchical ranking strategy to evaluate and prioritize SWAP candidates, as shown in Fig. 4(c).

- **Level-1 Distance Cost.** Following the *SABRE* heuristic, MERA computes a weighted distance cost based on the current 2Q interaction and a *look_ahead* window of upcoming 2Q gates. The accumulated distance serves as the primary ranking metric, favoring candidates that reduce near-term routing overhead.
- **Level-2 MCM-Error.** For candidates whose Level-1 scores lie within the Δ_{swap} range, MERA further ranks SWAPs by the product of the post-swap physical qubit’s MCM error rate and the logical qubit’s remaining MCM intensity after routing. The lowest-product candidate is selected, preventing high-intensity logical qubits from mapping to high-error physical qubits.

As shown in Fig. 4(c), qubit q_2 with more MCM operations must interact with q_4 via a 2Q gate. A SWAP can occur between $q_2 - q_3$ or $q_3 - q_4$. The latter is selected because it prevents the MCM-intensive qubit q_2 from being relocated to a physical qubit with higher MCM-error rates. Additional MCM operations on q_2 are omitted for brevity but explained in the caption of Fig. 4.

D. Scheduling Stage

After routing, MERA applies an as-late-as-possible (ALAP) scheduler to compact gate execution and explicitly expose idle intervals. A Context-Aware Dynamic Decoupling (CADD) module then inserts decoupling pulses only within these ALAP-generated delay windows to suppress decoherence.

Unlike conventional DD, CADD adapts its pulse placement to circuit context, including MCM timing and qubit-dependent noise, thereby avoiding MCM windows and minimizing interference with subsequent gates. By coordinating pulse timing across coupled qubits, CADD also mitigates the ZZ crosstalk that dominates during MCM operations [11]. As illustrated in Fig. 4(d), ALAP creates a delay window on q_1 during the MCM on q_2 , while q_3 and q_4 are shifted rightward so that their final H and CX gates align with the end of the MCM window. Consequently, CADD inserts $X-X$ sequences only on q_1 , with no need for DD on q_3 or q_4 . By combining ALAP scheduling with CADD, MERA provides fine-grained noise suppression tailored to MCM-induced idle behavior.

TABLE I: Parameter settings for the implementation of MERA.

Notation	Description	Values
τ_{MCM}	Threshold of MCM error rate in Eq. (2).	0.02
$[\alpha, \beta, \gamma, \delta, \epsilon]$	Weights for scoring the seed qubit in Eq. (3).	[0.25, 0.25, 0.1, 0.2, 0.2]
N_{Seed}	Number of selected seed qubits.	4
$look_ahead$	Number of look ahead layers in Eq. (4).	6
$w_{dist/MCM/2Q/1Q/RO}$	Weights for the cost function in Eq. (4).	[0.45, 0.2, 0.2, 0.05, 0.1]
Δ_{swap}	Threshold for determining next swap.	0.008

V. EVALUATION

A. Evaluation Setup

Implementations. We implemented MERA using Python 3.11.13 and Qiskit v2.1.2. The parameter settings described in Sec. IV are listed in Table I. These parameter values were determined through grid-search tuning over the benchmarks in our evaluation, selecting the configuration that achieved the highest overall fidelity.

Baselines. We use the Qiskit-compiler (v2.1.2) as a baseline, which does not model MCM errors. Two Qiskit settings are evaluated: Qiskit -O3 (optimization level 3) and Qiskit -WM (worst mapping under optimization level 3), which constrains the layout to a contiguous physical subgraph with the highest cumulative MCM cost (MCM-intensity \times MCM-error) from the measured MCM distribution. We also include QR-Map [17], a SOTA qubit-reuse compiler, to assess fidelity gains when MERA post-processes its outputs.

Evaluation Platforms. We conduct the evaluations in Sec. V-B and V-C using a 127-qubit heavy-hex simulator that replicates the IBM Eagle coupling map and incorporates all noise parameters, including MCM error rates, extracted from the calibration data in Sec. III. The simulator is implemented with Qiskit’s AerSimulator in “statevector” mode to support dynamic circuits, with CX as the native two-qubit gate. For real-device evaluation (Sec. V-D), we use the 127-qubit IBM Eagle and 156-qubit IBM Heron processors.

Benchmarks. We select 27 benchmarks for evaluation, including 8 RUS benchmarks with qubit counts from 4 to 18. A 4-qubit RUS benchmark used in our evaluation is illustrated in Fig. 1b. All 8 RUS benchmarks are designed to place 2Q gates on adjacent qubits (e.g., q_1-q_2, q_3-q_4, \dots) before and after the RUS segment, ensuring no SWAPs are needed under proper layouts, therefore making MCM-induced fidelity loss directly observable by isolating SWAPs. Additionally, our evaluation includes 6 qubit-reuse circuits from [3], 2 MCM-containing benchmarks from QASMBench [20], and 11 qubit-reuse circuits generated by QR-Map [17].

Evaluation Metrics. For each benchmark, we run 1,024 shots per iteration and repeat each benchmark for five iterations. For RUS circuits, we define the **Attempts** metric as the total number of MCM operations required for the circuit to reach success across all $5 \times 1,024$ shots (**for RUS circuits only**); lower values of Attempts indicate higher success rates. For all benchmarks, the average execution fidelity (**Fidelity**) is measured using Hellinger fidelity [16]. We also adopt two metrics from prior work [3], [17], [12] – the average number of

TABLE II: Evaluation results of qubit-reuse and QASMBench benchmarks. In the “Qubits” column, $m - n$ denotes circuits with m logical qubits mapped to n physical qubits after reuse.

Bench	Qubits	MERA -w CADD		MERA -w/o CADD		Qiskit -O3		Qiskit -WM					
		Path	SWAP Fidelity	Path	SWAP Fidelity	Path	SWAP Fidelity	Path	SWAP Fidelity				
BV	4-2	20	0	0.95	20	0	0.93	20	0	0.69	20	0	0.34
	7-2	38	0	0.89	38	0	0.88	38	0	0.53	38	0	0.13
	10-2	63	0	0.86	63	0	0.83	63	0	0.42	63	0	0.04
H-Ladder	3-2	24	0	0.96	24	0	0.95	24	0	0.75	24	0	0.45
	5-2	40	0	0.93	40	0	0.91	40	0	0.61	40	0	0.22
	7-2	56	0	0.88	56	0	0.87	56	0	0.50	56	0	0.10
IPEA	2	37	0	0.91	37	0	0.91	37	0	0.61	37	0	0.26
	Shor5	5	89	7	0.98	89	7	0.98	89	7	0.98	89	7

TABLE III: Fidelity comparison with QR-Map. The “Qubits” column also uses $m - n$ to denote circuits with m logical qubits mapped to n physical qubits after reuse.

Bench	Qubits	MERA -w CADD			MERA -w/o CADD			QR-Map		
		Path	SWAP	Fidelity	Path	SWAP	Fidelity	Path	SWAP	Fidelity
QAOA	10-6	79	18	0.56	79	18	0.55	79	18	0.53
	20-10	145	61	8e-5	145	61	8e-5	145	61	5e-5
QAOA-L2	10-7	139	25	0.57	139	25	0.52	139	25	0.50
QAOA-L3	10-9	167	49	0.51	167	49	0.49	167	49	0.48
RD-32	4-3	41	3	0.95	41	3	0.93	41	3	0.84
4MOD5	5-3	31	4	0.94	31	4	0.91	31	4	0.86
XOR_5	6-2	10	0	0.93	10	0	0.92	10	0	0.75
BV_10	10-2	63	0	0.86	63	0	0.84	63	0	0.67
SYM_9	12-5	392	72	0.69	392	72	0.63	392	72	0.31
MUL_13	13-7	129	32	0.61	129	32	0.60	129	32	0.50
QRAM	20-13	395	180	0.21	395	180	0.18	395	180	0.18

inserted SWAPs (**SWAP**) and the average critical path length (**Path**) – to quantify compilation overhead.

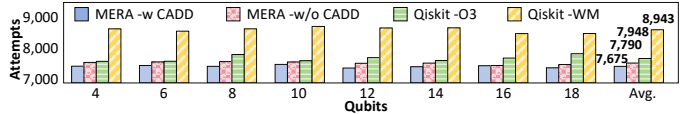
B. Comparision with Qiskit-Compiler

RUS Benchmarks. As shown in Fig. 6b, MERA with CADD consistently outperforms Qiskit -O3 and Qiskit -WM across all eight RUS benchmarks, achieving fidelity improvements of 6.90%–65.52% (average 24.94%) over Qiskit -O3, while requiring fewer attempts (Fig. 6a) and introducing neither extra SWAPs nor longer critical paths. Even without CADD, MERA still delivers an average fidelity gain of 22.81%, underscoring the effectiveness of MCM-aware layout and routing. Under Qiskit’s worst-case layout (-WM), attempts increase sharply and fidelity collapses, highlighting the strong impact of MCM errors on RUS circuits.

Qubit-Reuse and QASMBench Benchmarks. Table II presents results on six qubit-reuse circuits and two QASMBench benchmarks. MERA, with and without CADD, achieves average fidelity improvements of 52.00% and 49.68% over Qiskit -O3, respectively, and consistently surpasses Qiskit -WM across all cases without adding SWAPs. In the Shor5 benchmark, where only two MCM operations occur, MERA shows limited improvement over Qiskit -O3, indicating that its benefits are more pronounced for circuits with higher MCM intensity, such as RUS and qubit-reuse circuits.

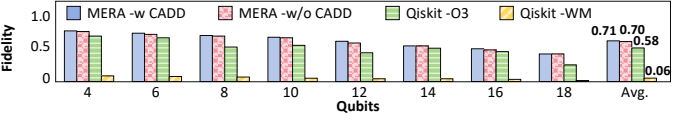
C. Improvements over QR-Map

We use MERA to post-process 11 qubit-reuse circuits originally generated by QR-Map. As shown in Table III, for the

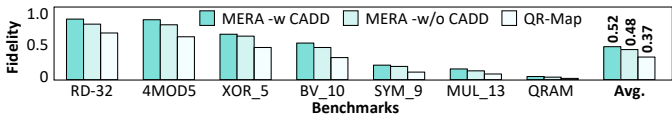


(a) Comparison of the **Attempts** metric. **Lower is better.**

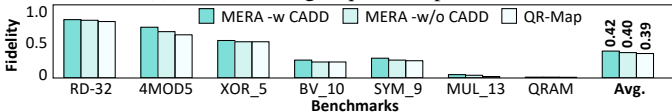
Fig. 6: Evaluation results of eight RUS benchmarks. Note that the average critical depth (**Path** = 28) and average number of inserted SWAP gates (**SWAP** = 0) are **identical** for MERA and Qiskit under different options, and thus omitted for brevity.



(b) Comparison of the **Avg. Fidelity** metric. **Higher is better.**



(a) The IBM Eagle quantum processor.



(b) The IBM Heron quantum processor.

Fig. 7: Fidelity evaluation of benchmark circuits on real devices (127-qubit IBM Eagle and 156-qubit IBM Heron).

SYM_9 benchmark, MERA achieves fidelity improvements of 122.58% (with CADD) and 103.23% (without CADD). Two larger benchmarks (QAOA 20-10 and QRAM 20-13) are included to assess scalability, though their fidelities remain low due to their larger qubit counts. Overall, MERA achieves average improvements of 29.26% with CADD and 23.42% without CADD over QR-Map. These results underscore the effectiveness of MCM-error-aware layout and routing in improving the reliability of qubit-reuse circuits. Importantly, MERA is orthogonal to existing compilation frameworks, including distributed, quantum error correction, and qubit-reuse compilers, and can serve as an add-on module to further improve fidelity in any compiler workflow involving MCM operations. Notably, MERA's compilation runtime ranges from 0.12 to 0.77 seconds on 11 benchmarks, indicating that it introduces no significant runtime overhead.

D. Real-Device Evaluation

To evaluate the scalability of MERA, we conducted real-device experiments on the 127-qubit IBM Eagle and 156-qubit IBM Heron processors using 7 benchmark circuits adopted in the real-device evaluation in QR-Map [17]. As shown in Fig. 7a, MERA achieves an average fidelity improvement of 40.55% over QR-Map with CADD and 39.73% without CADD across all benchmarks on Eagle. This fidelity gain demonstrates MERA's scalability and effectiveness. On the Heron processor (Fig. 7b), MERA also outperforms QR-Map on all benchmarks, but the gains are noticeably smaller (averaging 7.69% with CADD and 2.56% without CADD). The smaller gain arises from Heron's substantially lower MCM error rates compared to Eagle (as shown in Fig. 2), leaving limited room for MCM-aware layout and routing to further improve fidelity.

E. Discussion

Evaluation shows that MERA effectively improves benchmark fidelity by mitigating MCM-induced crosstalk, decoherence, readout error, and qubit-dependent reset infidelity. However, our current MCM-error model considers only $|1\rangle \rightarrow |0\rangle$ reset transitions; practical resets also suffer from leakage to higher energy levels, which should be addressed through hardware mechanisms rather than the compiler [24]. Likewise, MERA treats readout error only as a cost term, whereas additional mitigation can be achieved via hardware- or protocol-level methods [33], [32], [19]. Future work should integrate hardware leakage suppression, MERA, and dedicated readout-error mitigation to further reduce overall MCM-related errors.

VI. RELATED WORK

Quantum Compilers. Quantum compilers [6], [22], [15], [12], [13], [17], [23], [30] translate abstract algorithms into quantum circuits through techniques such as gate fusion, re-synthesis, and error mitigation. Compilers like Pauliheiral [22] enhance noise suppression, while CAQR [12] and QR-Map [17] exploit qubit reuse for better resource utilization. In contrast, MERA targets MCM error mitigation, distinguishing it from existing quantum compilers.

Quantum Error Mitigation. A broad range of methods address NISQ noise and perform quantum error correction across many error sources, across different error sources and platforms [28], [33], [32], [31], [27], [5]. Specifically, several studies characterize MCM errors [11], [9], [3], [19], but none incorporate them into the compilation process. MERA fills this gap by performing MCM-error-aware compilation.

VII. CONCLUSION

This paper presents MERA, a compilation framework that incorporates MCM error awareness into layout, routing, and scheduling. With lightweight profiling, MERA captures a stable per-qubit MCM error distribution that persists for over 24 hours. Leveraging these profiled distributions and CADD to mitigate MCM errors, MERA improves circuit fidelity and achieves substantial average gains over the Qiskit-compiler and QR-Map across 27 benchmarks, proving its effectiveness for circuits involving frequent MCM operations.

REFERENCES

- [1] Seif Alireza, Liao Haoran, Tripathi Vinay, Krsulich Kevin, Malekakhlagh Moein, Amico Mirko, Jurcevic Petar, and Javad Abhari Ali. Suppressing Correlated Noise in Quantum Computers via Context-Aware Compiling. In 2024 ACM/IEEE 51st Annual International Symposium on Computer Architecture (ISCA), pages 310–324, Buenos Aires, Argentina, 2024. IEEE Press.

[2] Ethan Bernstein and Umesh Vazirani. Quantum complexity theory. *SIAM Journal on Computing*, 26(5):1411–1473, 1997.

[3] Sebastian Brandhofer, Ilia Polian, and Kevin Krsulich. Optimal Qubit Reuse for Near-Term Quantum Computers . In *2023 IEEE International Conference on Quantum Computing and Engineering (QCE)*, pages 859–869, Los Alamitos, CA, USA, September 2023. IEEE Computer Society.

[4] Yudong Cao, Jonathan Romero, Jonathan P. Olson, Matthias Degroote, Peter D. Johnson, Mária Kieferová, Ian D. Kivlichan, Tim Menke, Borja Peropadre, Nicolas P. D. Sawaya, Sukin Sim, Libor Veis, and Alán Aspuru-Guzik. Quantum Chemistry in the Age of Quantum Computing. *Chemical Reviews*, 119(19):10856–10915, 2019. PMID: 31469277.

[5] Cheng Chu, Nai-Hui Chia, Lei Jiang, and Fan Chen. Qmlp: An error-tolerant nonlinear quantum mlp architecture using parameterized two-qubit gates. In *Proceedings of the ACM/IEEE International Symposium on Low Power Electronics and Design*, ISLPED ’22, New York, NY, USA, 2022. Association for Computing Machinery.

[6] Yongshan Ding, Xin-Chuan Wu, Adam Holmes, Ash Wiseth, Diana Franklin, Margaret Martonosi, and Frederic T. Chong. SQUARE: Strategic Quantum Ancilla Reuse for Modular Quantum Programs via Cost-Effective Uncomputation. In *Proceedings of the ACM/IEEE 47th Annual International Symposium on Computer Architecture*, ISCA ’20, page 570–583, Virtual Event, 2020. IEEE Press.

[7] Daniel J. Egger, Claudio Gambella, Jakub Marecek, Scott McFaddin, Martin Mevissen, Rudy Raymond, Andrea Simonetto, Stefan Woerner, and Elena Yndurain. Quantum computing for finance: State-of-the-art and future prospects. *IEEE Transactions on Quantum Engineering*, 1:1–24, 2020.

[8] Google. Google Quantum Computer. <https://quantumai.google/quantumcomputer>, 2025.

[9] L Góvia, P Jurecic, Christopher Wood, N Kanazawa, S Merkel, and D McKay. A Randomized Benchmarking Suite for Mid-Circuit Measurements. *New Journal of Physics*, 25, 12 2023.

[10] Aram W. Harrow, Avinatan Hassidim, and Seth Lloyd. Quantum Algorithm for Linear Systems of Equations. *Phys. Rev. Lett.*, 103:150502, Oct 2009.

[11] Daniel Hothem, Jordan Hines, Charles Baldwin, Dan Gresh, Robin Blume-Kohout, and Timothy Proctor. Measuring Error Rates of Mid-circuit Measurements. *Nature Communications*, 16, 07 2025.

[12] Fei Hua, Yuwei Jin, Yanhao Chen, Suhas Vittal, Kevin Krsulich, Lev S. Bishop, John Lapeyre, Ali Javadi-Abhari, and Eddy Z. Zhang. CaQR: A Compiler-Assisted Approach for Qubit Reuse through Dynamic Circuit. In *Proceedings of the 28th ACM International Conference on Architectural Support for Programming Languages and Operating Systems*, Volume 3, ASPLOS 2023, page 59–71, New York, NY, USA, 2023. Association for Computing Machinery.

[13] IBM. IBM Qiskit Transpiler. <https://quantum.cloud.ibm.com/docs/en/api/qiskit/transpiler#>, 2025.

[14] IBM. IBM Quantum Computing. <https://www.ibm.com/quantum>, 2025.

[15] Ali Javadi-Abhari, Shruti Patil, Daniel Kudrow, Jeff Heckey, Alexey Lvov, Frederic T. Chong, and Margaret Martonosi. ScaffCC: a Framework for Compilation and Analysis of Quantum Computing Programs. In *Proceedings of the 11th ACM Conference on Computing Frontiers*, CF ’14, New York, NY, USA, 2014. Association for Computing Machinery.

[16] Ali Javadi-Abhari, Matthew Treinish, Kevin Krsulich, Christopher J. Wood, Jake Lishman, Julien Gacon, Simon Martiel, Paul D. Nation, Lev S. Bishop, Andrew W. Cross, Blake R. Johnson, and Jay M. Gambetta. Quantum Computing with Qiskit, 2024.

[17] Hyungsik Kim, Enhyeok Jang, Seungwoo Choi, Youngmin Kim, and Won Woo Ro. QR-Map: A Map-Based Approach to Quantum Circuit Abstraction for Qubit Reuse Optimization. In *Proceedings of the 52nd Annual International Symposium on Computer Architecture*, ISCA ’25, page 1568–1582, New York, NY, USA, 2025. Association for Computing Machinery.

[18] Junpyo Kim, Dongmoon Min, Jungmin Cho, Hyeonseong Jeong, Ilkwon Byun, Junhyuk Choi, Juwon Hong, and Jangwoo Kim. A Fault-Tolerant Million Qubit-Scale Distributed Quantum Computer. In *ACM International Conference on Architectural Support for Programming Languages and Operating Systems*, ASPLOS ’24, page 1–19, New York, NY, USA, 2024. Association for Computing Machinery.

[19] Jin Ming Koh, Dax Enshan Koh, and Jayne Thompson. Readout Error Mitigation for Mid-Circuit Measurements and Feedforward, 2025.

[20] Ang Li, Samuel Stein, Sriram Krishnamoorthy, and James Ang. QASMBench: A Low-Level Quantum Benchmark Suite for NISQ Evaluation and Simulation. *ACM Transactions on Quantum Computing*, 4(2), February 2023.

[21] Gushu Li, Yufei Ding, and Yuan Xie. Tackling the Qubit Mapping Problem for NISQ-Era Quantum Devices. In *Proceedings of the Twenty-Fourth International Conference on Architectural Support for Programming Languages and Operating Systems*, ASPLOS ’19, page 1001–1014, New York, NY, USA, 2019. Association for Computing Machinery.

[22] Gushu Li, Anbang Wu, Yunong Shi, Ali Javadi-Abhari, Yufei Ding, and Yuan Xie. Paulihedral: a Generalized Block-Wise Compiler Optimization Framework for Quantum Simulation Kernels. In *Proceedings of the 27th ACM International Conference on Architectural Support for Programming Languages and Operating Systems*, ASPLOS ’22, page 554–569, New York, NY, USA, 2022. Association for Computing Machinery.

[23] Yuhao Liu, Shize Che, Junyu Zhou, Yunong Shi, and Gushu Li. Fermihedral: On the optimal compilation for fermion-to-qubit encoding. *ASPLOS*, 3(1):382–397, 2024.

[24] Matt McEwen, Dvir Kafri, Jimmy Chen, Juan Atalaya, Kevin Satzinger, Chris Quintana, Paul Victor Klimov, Daniel Sank, Craig Michael Gidney, Austin Fowler, Frank Carlton Arute, Kunal Arya, Bob Benjamin Buckley, Brian Burkett, Nicholas Bushnell, Benjamin Chiaro, Roberto Collins, Sean Demura, Andrew Dunsworth, Catherine Erickson, Brooks Riley Foxen, Marissa Giustina, Trent Huang, Sabrina Hong, Evan Jeffrey, Seon Kim, Kostyantyn Kechedzhi, Fedor Kostritsa, Pavel Laptev, Anthony Megrant, Xiao Mi, Josh Mutus, Ofer Naaman, Matthew Neeley, Charles Neill, Murphy Yuezhen Niu, Alexandru Paler, Nick Redd, Pedram Roushan, Ted White, Jamie Yao, Ping Yeh, Adam Jozef Zalcman, Yu Chen, Vadim Smelyanskiy, John Martinis, Hartmut Neven, J. Kelly, Alexander Korotkov, Andre Gregory Petukhov, and Rami Barends. Removing Leakage-induced Correlated Errors in Superconducting Quantum Error Correction. *Nature Communications*, 12:1761, 2021.

[25] Miguel Moreira, Gian Giacomo Guerreschi, Wouter Vlothuizen, J. F. Marques, J. van Straten, Shavindra P. Premaratne, X. Zou, H. Ali, Nandini Muthusubramanian, C. Zachariadis, J. van Someren, M. Beekman, N. Haider, Alessandro Bruno, Carmen Garcia Almudever, Anne Y. Matsuuura, and Leonardo DiCarlo. Realization of a Quantum Neural Network using Repeat-until-Success Circuits in a Superconducting Quantum Processor. *npj Quantum Information*, 9:1–7, 2022.

[26] John Preskill. Quantum Computing in the NISQ Era and Beyond. *Quantum*, 2:79, August 2018.

[27] Yosuke Ueno, Masaaki Kondo, Masamitsu Tanaka, Yasunari Suzuki, and Yutaka Tabuchi. *QECCOL: On-Line Quantum Error Correction with a Superconducting Decoder for Surface Code*, page 451–456. IEEE Press, San Francisco, CA, USA, 2022.

[28] Yosuke Ueno, Masaaki Kondo, Masamitsu Tanaka, Yasunari Suzuki, and Yutaka Tabuchi. Qulatis: A quantum error correction methodology toward lattice surgery. In *2022 IEEE International Symposium on High-Performance Computer Architecture (HPCA)*, pages 274–287, Seoul, South Korea, 2022. IEEE Press.

[29] Nathan Wiebe and Martin Roetteler. Quantum Arithmetic and Numerical Analysis using Repeat-until-Success Circuits. *Quantum Info. Comput.*, 16(1–2):134–178, January 2016.

[30] Xin-Chuan Wu, Dripto M. Debroy, Yongshan Ding, Jonathan M. Baker, Yuri Alexeev, Kenneth R. Brown, and Frederic T. Chong. TILT: Achieving Higher Fidelity on a Trapped-Ion Linear-Tape Quantum Computing Architecture . In *2021 IEEE International Symposium on High-Performance Computer Architecture (HPCA)*, pages 153–166, Los Alamitos, CA, USA, March 2021. IEEE Computer Society.

[31] Bo Yang, Rudy Raymond, and Shumpei Uno. Efficient quantum readout-error mitigation for sparse measurement outcomes of near-term quantum devices. *Phys. Rev. A*, 106:012423, Jul 2022.

[32] Hanyu Zhang, Liqiang Lu, Siwei Tan, Size Zheng, Jia Yu, and Jianwei Yin. SpREM: Exploiting Hamming Sparsity for Fast Quantum Readout Error Mitigation. In *Proceedings of the 61st ACM/IEEE Design Automation Conference*, DAC ’24, New York, NY, USA, 2024. Association for Computing Machinery.

[33] Kaiwen Zhou, Liqiang Lu, Hanyu Zhang, Debin Xiang, Chennng Tao, Xinkui Zhao, Size Zheng, and Jianwei Yin. DyREM: Dynamically Mitigating Quantum Readout Error with Embedded Accelerator. In *2025 62nd ACM/IEEE Design Automation Conference (DAC)*, pages 1–7, San Francisco, CA, USA, 2025. IEEE Press.